NUMERICAL INVESTIGATION ON THE CONVECTIVE HEAT TRANSFER IN A SPIRAL COIL WITH RADIANT HEATING

by

Milan Lj. DJORDJEVIĆ [a*], Velimir P. STEFANOVIĆ [b], Mića V. VUKIĆ [b], and Marko V. MANČIĆ [b]

[a] Faculty of Technical Sciences, University of Pristina, Kosovska Mitrovica, Serbia
[b] Faculty of Mechanical Engineering, University of Nis, Nis, Serbia

Original scientific paper
DOI: 10.2298/TSCI16S5215D

The objective of this study was to numerically investigate the heat transfer in spiral coil tube in the laminar, transitional, and turbulent flow regimes. The Archimedean spiral coil was exposed to radiant heating and should represent heat absorber of parabolic dish solar concentrator. Specific boundary conditions represent the uniqueness of this study, since the heat flux upon the tube external surfaces varies not only in the circumferential direction, but also in the axial direction. The curvature ratio of spiral coil varies from 0.029 at the flow inlet to 0.234 at the flow outlet, while the heat transfer fluid is water. The 3-D steady-state transport equations were solved using the Reynolds stress turbulence model. Results showed that secondary flows strongly affect the flow and that the heat transfer is strongly asymmetric, with higher values near the outer wall of spiral. Although overall turbulence levels were lower than in a straight pipe, heat transfer rates were larger due to the curvature-induced modifications of the mean flow and temperature fields.

Key words: *Archimedean spiral coil, heat transfer, numerical simulation*

Introduction

The utilization of modern paraboloidal concentrators for conversion of solar radiation into heat energy requires the development and implementation of compact and efficient heat absorbers (HA). Knowledge of the distribution of radiant heat flux incident upon the absorber tubes at any point along their length and circumference will aid in developing meaningful heat transfer information for the absorber. The radiant heat flux field is incident on only one-half of the circumference of the absorber tubes in parabolic dish receivers. This investigation is focused on the heat transfer characteristics of Archimedean spiral coil employed as HA in parabolic dish receiver.

Spiral tubes or spiral coils were introduced in 19th century and have been widely used in various thermal engineering applications, such as heat exchangers, electronic cooling, chemical reactors, *etc.* They have better heat transfer performance and compactness in comparison with commonly used straight tube exchangers, which results in occupying less space. The transport phenomena occurring in the spiral tubes are more complicated than those in straight tubes. Secondary flows observed in the flow patterns, induced by centrifugal force, significantly affect the flow field and heat transfer.

* Corresponding author; e-mail: milan.djordjevic@pr.ac.rs

Convective heat transfer and flow developments in the curved tube strongly depend on the behavior of secondary flow. The secondary flow in the curved tube is caused by the centrifugal force. This force has significant effect on the enhancement of heat transfer. The enhancement of heat and mass transfer in curved geometries is due to the onset of secondary flow structures which appear as twin counter rotating vortices in the cross-sectional plane. Consequently the fluid in the central region is driven toward the outer wall by centrifugal force and this phenomenon, by causing the thinning of the boundary layer, necessarily encourages the heat transfer mechanism.

A mathematical model for the fluid flow in a toroidal duct of constant radius was introduced by Dean [1, 2]. His studies revealed that a secondary flow develops in curved tubes when so called the Dean number exceeds a certain critical value. A characteristic secondary motion develops in the cross-section due to the imbalance between pressure and inertial forces [1]. The fluid moves towards the outer bend side near the equatorial mid-plane, returns towards the inner side along two near-wall boundary layers, thus forming two symmetric secondary cells having a characteristic velocity scale $V_{av}\delta^{0.5}$.

Since then, several experimental [3-8] and numerical [9-16] studies have been published, which examined the flow and heat transfer phenomena in the spiral tubes. Most of these papers investigate laminar flow of Newtonian fluids in coils, while those that investigate turbulent flow conditions are rare. Moreover, all take into account two common thermal boundary conditions – constant wall temperature and constant heat flux.

Even though the interest in spiral coiled systems is on the rise, there are still very few published articles on spiral coil tubes. They are less popular compared to helical tubes, which have attracted major attention in the study of coiled tubes for heat transfer. There is very little information and correlations on the Nusselt number, and in the absence of appropriate correlations, traditional approach is to use correlations developed for circular or helical tubes with an average curvature.

Earlier investigations have shown that the presence of centrifugal force due to curvature will lead to significant radial pressure gradient in the flow core region [17]. In the proximity of curved ducts inner and outer walls, however, the axial velocity and the centrifugal force will approach zero. Hence, to balance the momentum transport, secondary flows will appear. Due to the curvature and no slip boundary condition at the spiral walls, the development of axial velocity is affected by the axial and secondary flows. The numerical simulation results indicate that the axial flow pattern is different for low and high Reynolds numbers depending on the spiral tube configuration, thereby affecting the temperature field.

There is the similarity of flow phenomena between heated straight pipes and unheated curved pipes, the techniques developed in treating the flow problem in the latter can be applied to study the flow development in the former. Morton [18] found that the flow in a heated straight pipe is similar to that in a curved pipe. Heated pipes also develop vortices that result from the combination of the radial-directional and the downward motions of the fluid particles which are induced by the displacement of the boundary layer and develop along the pipe. A favorable pressure gradient is generated on the bottom wall of the pipe, while an unfavorable pressure gradient is induced on the top wall. Natural convection and variable material properties play important roles in the heat transfer and fluid flow in a heated pipe. Frequently the prediction of the heat transfer by forced convection alone, without considering the secondary flow induced by buoyancy force, could cause significant errors, especially for laminar flow cases.

Another interesting character of the flow in heated pipes, revealed by Mori *et al.* [19], is that the secondary flow generated by heating can suppress the turbulence level when

the inlet turbulence level is high and can enhance it when its level is low at the inlet. On the other hand, the curvature of the wall stabilizes the flow by delaying the transition to the turbulent flow. The effect of the inertia forces, which act on the fluid's particles due to the curvature of the trajectories that they are forced to follow, has a positive effect on the convective heat transfer coefficient.

Geometric, mathematical and numerical model

The objective of this paper was to study numerically the distribution of the convective heat transfer in a horizontal spiral-coil tube exposed to radiant heating that is characteristic of parabolic dish solar concentrators. The Archimedean spiral, with the pitch slightly larger than the outside diameter of the smooth coiling tube, was selected between different types of spirals in order to achieve the most favorable ratio of active surface area and the total volume of the HA in parabolic dish receiver. Geometrical parameters of analyzed Archimedean spiral coil heat absorber are listed in tab. 1, while the geometric model of the spiral coil and receiver cavity is shown in fig. 1.

Table 1. Geometrical parameters of HA

Archimedean spiral coil			
d_i	11.7	mm	inside diameter of pipe
d_o	12.2	mm	outside diameter of pipe
s	0.25	mm	pipe wall thickness
R_{min}	25	mm	minimum radius of the coil
R_{max}	202	mm	maximum radius of the coil
p_s	13.6	mm	spiral coil pitch
n	13	–	number of coil turns

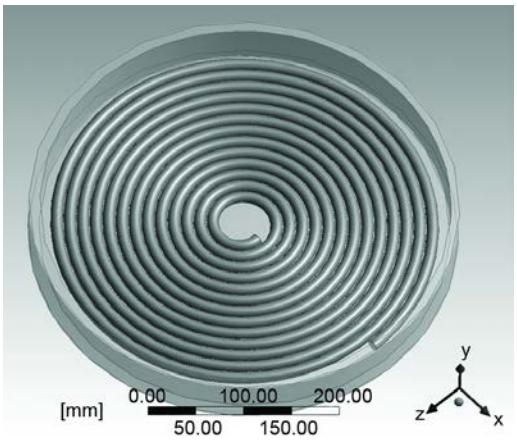

Figure 1. Geometric model of spiral coil heat absorber positioned in the receiver cavity

From the geometry of the spirally coiled test section, it is obvious that only one-half of the perimeter of each turn cross section receives the incident radiation and the other half remains in the shadow and will not see the radiation source. As the incident radiation is not uniform in the focal plane (where the HA is placed), the heat flux upon the tube external surfaces will vary not only in the circumferential direction, but also in the axial direction. The incident heat flux distribution in the focal plane is shown in fig. 2 [20], where z is the radial distance from the center of the plane.

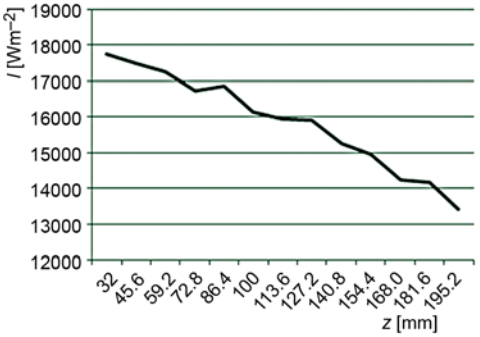

Figure 2. Incident flux distribution in the focal plane

The incident heat flux distribution on outside surface of spirally coiled heat absorber was obtained by detailed 3-D numerical procedure in ANSYS FLUENT 15 using S2S Hemicube method. From the theoretical point of view, the circumferential distribution of the incident heat flux should be represented by a cosine function. The numerical simulations have shown that part of the reflected radiation from

adjacent tubes was also absorbed by the tube surface, which rendered the distribution of incident flux around the tube cross section more uniform.

Since the temperature of the air enclosed in the receiver cavity that surrounds the HA is higher than the temperature of HA (for considered horizontally placed spiral coil), the convective heat transfer on the outside wall of HA was also taken into account and calculated. This convective gains were added to incident radiation heat flux to obtain total heat flux distribution on the outside surface of the HA. The calculated portion of convective gains was less than 7% of the amount of heat that was theoretically added to transport fluid (for considered conditions).

Mathematical model

The following set of partial differential equations for velocity components, pressure and temperature as functions of *x*, *y*, *z* describes the turbulent flow and temperature field inside a spirally coiled heat absorber. The conservation equations are formulated in the Cartesian coordinate system because the applied flow solver (ANSYS FLUENT 15.0) uses the Cartesian system to formulate the conservation equations for all quantities.

The continuity equation is formulated in the following manner:

$$\frac{\partial}{\partial x_i}(\rho U_i) = 0 \tag{1}$$

The following equation system is the representation of the momentum equations in Cartesian co-ordinate system where $i, j \in \{1, 2, 3\}$:

$$\frac{\partial}{\partial x_i}(\rho U_j U_i) - \frac{\partial}{\partial x_i}\left[\mu\left(\frac{\partial U_j}{\partial x_i} + \frac{\partial U_i}{\partial x_j}\right)\right] = -\frac{\partial P}{\partial x_j} - \frac{\partial}{\partial x_i}\left(\rho\overline{u_i u_j}\right) + \rho F_{j-\text{body}} \tag{2}$$

The following form of the energy equation is solved to calculate the temperature field:

$$\frac{\partial}{\partial x_i}(\rho c_p U_i T) = \frac{\partial}{\partial x_j}\left(\lambda\frac{\partial T}{\partial x_j}\right) - \frac{\partial}{\partial x_j}\left(\rho c_p\overline{\varphi u_j}\right) \tag{3}$$

The transport equations have been formulated in a conservative form according to Patankar [21]. Body forces, including centrifugal and buoyancy force, are stated in form of source terms in the momentum equations and should be modeled with great care in present case. Temperature dependency of physical properties of the working fluid has been considered to improve the accuracy of the calculations. Interpolation polynomials used in the numerical calculations have been fitted to the available data of the physical properties of the water. The results presented are in terms of the local mixed mean temperature, or bulk temperature, variation along the spiral coil. The bulk temperature is given by [22]:

$$T_\text{b} = \frac{1}{VA_\text{c}}\int_{A_\text{c}} T\vec{\text{U}}\text{d}A \tag{4}$$

where V is the mean velocity given by:

$$V = \frac{1}{A_\text{c}}\int_{A_\text{c}} \vec{\text{U}}\text{d}A_\text{c} \tag{5}$$

The local internal heat transfer coefficient and local Nusselt number at any axial location z and peripheral position θ were then calculated from:

$$h_{\mathrm{i}}|_{z,\theta} = \frac{q_{\mathrm{i}}|_{z,\theta}}{T_{\mathrm{i}}|_{z,\theta} - T_b|_z} \tag{6}$$

$$\mathrm{Nu}|_{z,\theta} = \frac{h_{\mathrm{i}}|_{z,\theta}\, d_{\mathrm{i}}}{\lambda|_z} \tag{7}$$

Constitutive relations

Thermophysical properties of water are treated as temperature-dependent and were obtained as polynomial functions of temperature. The density, viscosity, thermal conductivity and specific heat capacity of water were described as [23]:

$$\rho(t) = 998.25 - 0.123261t - 0.00131119t^2 - 0.0000121406t^3 \tag{8}$$

$$\mu(t) = 0.00166167 - 0.0000410857t + 4.64802\cdot 10^{-7}t^2 - 1.90559\cdot 10^{-9}t^3 \tag{9}$$

$$\lambda(t) = 0.568733 + 0.00196461t - 9.77855\cdot 10^{-6}t^2 + 1.2432\cdot 10^{-8}t^3 \tag{10}$$

$$c_p(t) = 4222.62 - 0.694932t + 0.00624126t^2 + 8.29448\cdot 10^{-6}t^3 \tag{11}$$

Stability criteria for flow in spiral coil

The transition from laminar to turbulent flow in curved pipes occurs at higher critical Reynolds number than in straight pipes. The spiral coil flow is characterized by two critical Reynolds numbers, the first one when the turbulence has set only in the outer turns with lowest curvature ratio, and the second one, when the inertia forces, even in the innermost turns with highest curvature ratio, are sufficient to overcome the damping effect of the secondary flows. When fluid enters the coil from the outmost turn, the initial straight tube turbulence in the feed line gets damped out in the inner turns as the intensity of secondary circulation increases and only one transition takes place. At the approach of the first critical Reynolds number turbulence appears at the maximum radius point of the coil, and spreads to greater length with the further increase in Reynolds number. The following equations were used to estimate critical Reynolds numbers in smooth spiral [24]:

$$\mathrm{Re}_{\mathrm{crit}\ I} = 2100\left[1 + 4.9\left(\frac{d_{\mathrm{i}}}{R_{\max}}\right)^{0.21}\left(\frac{p}{R_{\max}}\right)^{0.1}\right] \tag{12}$$

$$\mathrm{Re}_{\mathrm{crit}\ II} = 2100\left[1 + 6.25\left(\frac{d_{\mathrm{i}}}{R_{\min}}\right)^{0.17}\left(\frac{p}{R_{\min}}\right)^{0.1}\right] \tag{13}$$

Applying eqs. (12) and (13), the values of critical Reynolds numbers in studied geometry (tab. 1) are: $\mathrm{Re}_{\mathrm{crit}\ I} = 6450$, and $\mathrm{Re}_{\mathrm{crit}\ II} = 13030$.

In this study all three flow cases were investigated, laminar, transitional and turbulent. Chosen Reynolds numbers corresponding these flow regimes are 3630, 7420, and 13050,

respectively. These values were obtained using thermophysical properties of water at average temperature $T_{av} = (T_{in} + T_{out})/2$ for particular flow regimes.

Description of numerical approach

Piazza and Ciofalo [25] applied the ANSYS CFX code to turbulent flow and heat transfer in curved pipes with zero torsion. Different turbulence models were used and compared, including the standard k-ε with wall functions, the SST k-ω and a second-order Reynolds stress model (RSM). The RSM model was found to yield the best agreement with experimental results.

The linear pressure-strain RSM was used within this investigation. Since the RSM was applied to near-wall flows using the enhanced wall treatment, the acceptance of low Reynolds number modifications to the linear pressure-strain model was needed. Pressure-strain rate correlations, or redistribution terms, were modeled with great care in this model. The exact formulation of the model and the values of the constants could be found in the literature [26, 27].

A fine structured mesh is applied near the wall and an increasingly coarser unstructured mesh in the middle of the channel in order to reduce the computational cost. Description of the entire geometry of the studied problem is incorporated into the generated hybrid numerical grid. The applied grid is strongly non-uniform near the wall of the tube to resolve the wall boundary effects. A careful check for the grid-independence of the numerical solutions has been made to ensure the accuracy and validity of the numerical scheme. Numerical calculations indicated that the value of curvature ratio δ ($\delta = d_i/D_c$) is the most critical for turbulence model validation, because the largest discrepancies from correlation data are obtained for the highest curvature. The outlet bulk temperature and the peripherally averaged Nu number on the 12th coil turn ($\delta = 0.2577$) have been used to test the independency of the calculation results from the applied grids (results are reported in tab. 2). The calculations have been carried out on four different grids and the relative errors of the control quantities were calculated. Initial and boundary conditions for the grid-independence tests of the smooth Archimedean spiral coil are formulated as follows: $V_{in} = 1.05$ ms^{-1}, $T_{in} = 20$ °C, $q_{wall} = 15{,}000$ Wm^{-2}, $(U, V, W)_{ini} = 0$ ms^{-1} and $T_{ini} = 20$ °C.

Table 2. Relative errors of the outlet bulk temperature and peripherally averaged Nu number

	Number of cells			
	(I) 6,351,164	(II) 7,213,902	(III) 8,628,928	(IV) 11,217,606
Outlet bulk temperature [°C]	24.84	24.76	24.73	24.71
Relative error of outlet temperature [%]	0.53	0.21	0.09	–
Average Nu number on 12th turn [–]	124.56	123.22	122.73	121.88
Relative error of Nu number [%]	2.2	1.1	0.7	–

It can be concluded that grid resolution larger than $8.6 \cdot 10^6$ cells (case III, second finest grid) in the studied geometry would be approximately enough to produce physically realistic results independent from the applied numerical grid. Selected grid is characterized by a geometric refinement introduced at the wall, with a wall normal expansion ratio 1.15 in the radial direction. The first near-wall grid points (volume centers) were at $y^+ = 0.23$ ($Re_{av} = 3630$), $y^+ = 0.56$ ($Re_{av} = 7420$), and $y^+ = 1$ ($Re_{av} = 13050$).

Selection of discretization schemes and algorithms was based on the extensive literature survey for numerical work dealing with similar problems. The momentum equations are discretized using the Power law [21]. Since the model considers both buoyancy and centrifugal source terms, pressure discretization is performed with body force-weighted approach. FLUENT uses the equation of continuity to deduce the pressure necessary to resolve the equations of motion. Due to the incompressible nature of the flow regimes, a direct link between the density and pressure is not obvious, and an algorithm is required to address an effective pressure-velocity coupling issue. The semi-implicit method for pressure-linked equations (SIMPLE) algorithm [21] is employed to introduce pressure into the continuity equation. The discretization and treatment of the continuity equation is an inherent choice from the software. The linearized set of equations was solved with a point implicit (Gauss-Seidel) solver in tandem with an algebraic multigrid (AMG) method. The convergence is achieved with values not higher than 10^{-3} for all variables and 10^{-6} for temperature.

A series of calculations were performed to investigate the validity of numerical computations for the smooth Archimedean spiral tube. Peripherally averaged local Nusselt numbers on each turn of the spiral have been calculated for constant flux boundary condition on the external surface of the tube. Results are compared with the famous Gnielinski modification of the Petukhov-Popov equation [28] for heat transfer in curved and helical pipes for the case Re_{av} = 13050 (fig. 3).

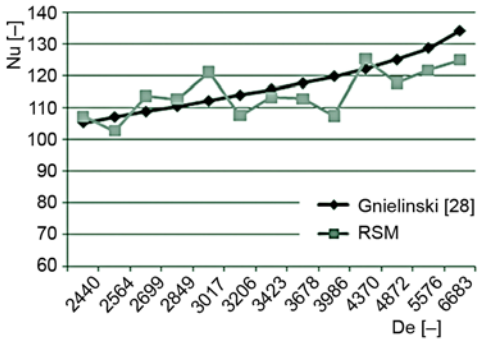

Figure 3. Comparison of the numerical results with analytical results (Re_{av} = 13050)

The numerically calculated results show good agreement with Gnielinski correlation, with an average deviation less than 2%. This could be explained by the fact that property variation of the water can modify the Prandtl number for about 12% between the inlet and outlet, while in the correlation the Nusselt numbers have been associated with the mean of the inlet and outlet value of the Prandtl number. On the other hand, fluid flow could not be regarded as fully developed in spiral coil, due to constantly varying curvature, while the Nu correlations were developed for constant curvature and fully developed turbulent flow.

Results and discussion

The cold water entering the outermost turn (1st turn) flows along the spiral tube and flows out at the outermost turn (13th turn). Constant mass flow is assumed at the inlet position of the heat absorber coil. The gradient of the velocity profile and of the temperature field is assumed to be zero at the inlet cross section. The heat flux profile on outside SURFACE of spiral coil heat absorber was obtained by detailed 3-D numerical procedure in FLUENT using S2S Hemicube method, as mentioned before, and was applied as boundary condition for al studied cases.

For the first of the numerical runs, the average Reynolds number (Re_{av} = 3630) was less than the first critical Reynolds number and only this one run was completely laminar throughout the spiral coil. For the second run, the average Reynolds number (Re_{av} = 7420) was between two critical Reynolds numbers, which meant that all three flow regimes (laminar, transitional and turbulent) should occur in the coil. The average Reynolds number

(Re_{av} = 13050) for the last run was greater than second critical Reynolds number, and this run was completely turbulent throughout the coil. The applied RSM model is able to predict laminarization at low Reynolds numbers, but prediction of the model in the transitional region could be less reliable, and should be taken with caution.

The local internal heat transfer coefficient and Nusselt number have been calculated at 13 axial locations that were positioned at the middle of each turn of the spiral in axial direction. At every axial location four peripheral locations were specified: location A (θ = 0°) corresponds to the outer side of the tube cross section (the furthest from the curvature center), location B (θ = 90°) corresponds to the side of the tube cross section which is directly subjected to radiant flux, location C (θ = 180°) corresponds to the inner side of the tube cross section (the closest to the curvature center) and location D (θ = 270°) which receives heat only by air convection and conduction through the tube wall. The heat flux at the inside wall of the pipe would be redistributed in relation to the absorbed radiant heat flux at the outside wall due to the significant circumferential wall temperature variations and conductance of the wall. The material of the wall is stainless still AISI 304.

The bulk temperature and local inside Nusselt numbers at predefined locations were calculated according to the above mentioned principles, eqs. (4)-(7), and shown in figs. 4-7. Fluid properties needed for evaluation of these variables were estimated at the local values of pressure and bulk temperature.

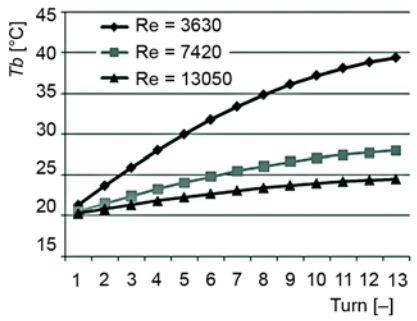

Figure 4. Axial distribution of bulk temperature

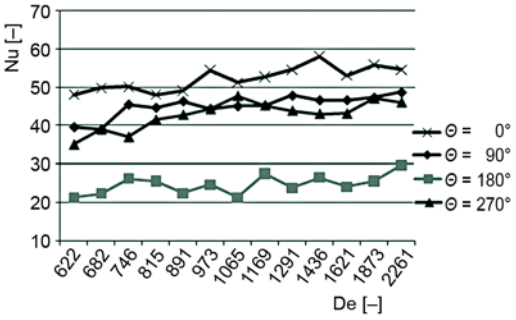

Figure 5. Axial distribution of Nusselt number at different peripheral locations, Re_{av} = 3630

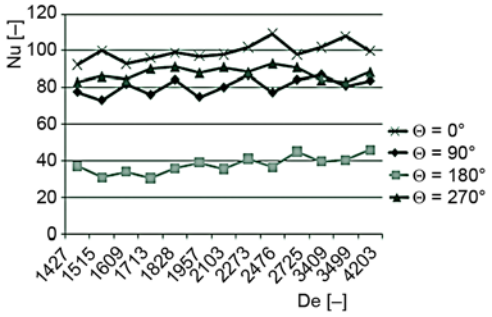

Figure 6. Axial distribution of Nusselt number at different peripheral locations, Re_{av} = 7420

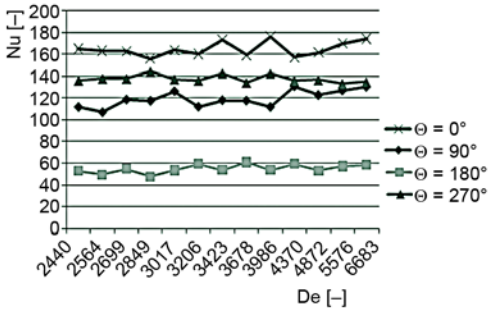

Figure 7. Axial distribution of Nusselt number at different peripheral locations, Re_{av} = 13050

Nusselt number fluctuates for observed range of curvature ratio, figs. (5)-(7), and this phenomenon is not characteristic of heat transfer in straight tubes. These oscillations are caused by the flow pattern, which is affected by the centrifugal, buoyancy and viscous forces. Combined effects of body and viscous forces induce formation of very complex thermal boundary layer. This is in accordance with previous findings of Seban and McLaughlin [29], who presented the experimental data on friction and heat transfer for the laminar flow of oil and the turbulent flow of water in curved pipes under the uniform wall heat flux boundary condition. Their data clearly showed an irregular behavior of the local convective heat transfer coefficient along the axial distance. Similar oscillatory behavior of the Nusselt number has also been found by Lin and Ebadian [30] in their numerical studies of turbulent convective heat transfer in smooth helical pipes.

Turbulent velocity and temperature fluctuations in curved pipes were much more intense in the outer region than in the inner one. With respect to the straight pipe case, velocity fluctuations were concentrated in a narrower near-wall layer and were relatively less intense in the core flow, while the temperature fluctuations in the core region were more intense. At the outlet region, where the radius of curvature decreases significantly with each turn, the flow stabilizes in relatively short distance, thus oscillations are not so significant. Increasing the curvature led to a decrease in the fluctuations of streamwise velocity, temperature and turbulent heat fluxes over the whole cross section.

The decrease of turbulence levels and turbulent heat fluxes with increasing the curvature ratio for a given Reynolds number might lead to conclusion that overall heat transfer rates would decrease. However, this is not the case, and the present computational results indicate a moderate but clear increase of the heat transfer coefficient with the increase of curvature ratio. Such behavior could be explained by the global changes that curvature induces in the flow and temperature fields, especially by pushing high-speed and low-temperature fluid towards the outer wall region and away from the inner wall. As a consequence, heat transfer increases in the outer region and decreases in the inner region quite independently on the changes in turbulence structure. The net effect is a slight increase of the average value of heat transfer, similarly as could be observed in laminar flow.

Peripherely averaged Nusselt numbers as a function of the curvature ratio δ at different Reynolds numbers are shown in fig. 8. The heat transfer generally increases along with the curvature ratio. It is noticeable that the increase of the Reynolds number reduces the impact of curvature ratio on the Nusselt number distribution. Numerical calculations show that the Nusselt number increases for 25.2% in laminar, 8.6% in transitional and 6.8% in fully turbulent flow regime in considered curvature ratio range.

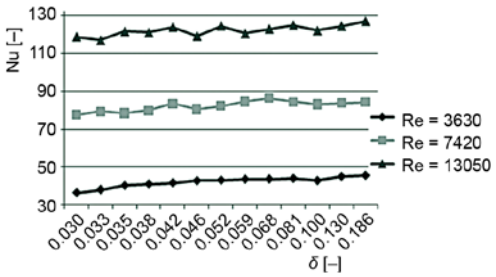

Figure 8. Peripherely averaged Nusselt numbers as a function of the curvature ratio

Local heat transfer results around the inner periphery of the pipe cross section at four coil turns (2^{nd}, 5^{th}, 9^{th}, and 12^{th}), and for different flow regimes were shown in figs. 9-11. These positions along the absorber were chosen such that each figure represents the circumferential variation of Nusselt number as the flow progresses through the spiral coil from inlet to exit.

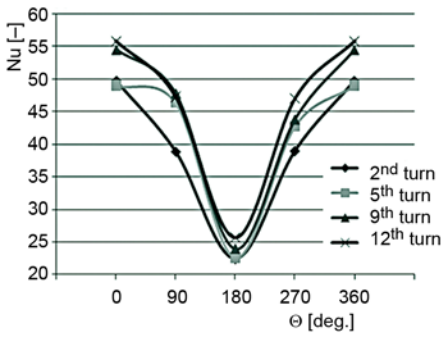

Figure 9. Circumferential distribution of Nusselt number, Re_{ave} = 3630

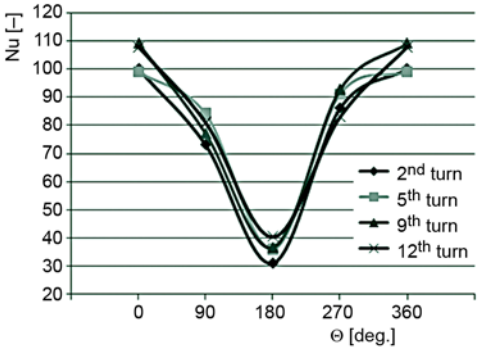

Figure 10. Circumferential distribution of Nusselt number, Re_{av} = 7420

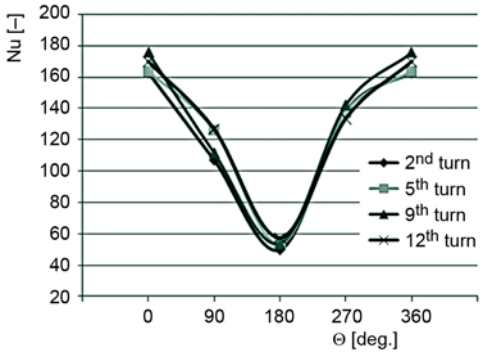

Figure 11. Circumferential distribution of Nusselt number, Re_{av} = 13050

The heat transfer from the walls are significantly affected by the secondary flow caused by the nature of the flow and constantly changing curvature, which results in not only axial but also circumferential boundary layer formations. The maximum velocity at the entrance region is observed to be at the center of curvature of the spiral tube, but further downstream the maximum velocity shifts towards the outer wall of the spiral tube. Well into the spiral tube, the fluid is heated more in regions where the velocity magnitude is less causing larger thermal boundary layers at the inner side of the spiral wall, while very thin thermal boundary layers are observed at the outer side of the spiral wall. Peripheral distribution of Nusselt number clearly indicate the presence of secondary circulation and strong stratification of streamwise velocity and temperature along the radius of curvature. This is characteristic both for laminar and turbulent flow.

Conclusion

The 3-D turbulent convective heat transfer in the Archimedean spiral coil tube under radiant heating has been studied numerically with control volume method. The numerical computations revealed the development and distribution of heat transfer in the spiral coil tube. The induced secondary flows by centrifugal and buoyancy forces in the coil tube with constantly changing curvature have significant effect on the enhancement of heat transfer. Results of numerical calculations with various inflow rates representing all three flow regimes indicate the development and distribution of the local Nusselt numbers at different axial and peripheral locations. The secondary flows strongly affect the flow, what in conjunction with specific boundary conditions, makes the heat transfer strongly asymmetric, with higher values near the outer wall of spiral and average values of Nusselt number significantly higher compared to the corresponding in straight tube. The local Nusselt numbers varies along the axial locations of spiral coil and this oscillating behavior is a consequence of the highly intensified secondary flow field.

Acknowledgment

The support of the Ministry of Education, Science and Technological Development of the Republic of Serbia through project 42006 is gratefully acknowledged.

Nomenclature

A_c – cross-section area, [m^2]
c_p – specific heat capacity, [kJkg^{-1}K^{-1}]
De – Dean number (= Re $\delta^{0.5}$), [–]
d_i – inside diameter of pipe, [m]
d_o – outside diameter of pipe, [m]
h_i – local value of inside heat transfer coefficient, [Wm^{-2}K^{-1}]
I – incident heat flux, [Wm^{-2}]
Nu – Nusselt number (= hd_i/λ), [–]
n – number of coil turns, [–]
P – pressure, [Pa]
p_s – spiral coil pitch, [m]
q_i – local value of heat flux at the inside surface of pipe, [Wm^{-2}]
Re – Reynolds number (= Vd/ν), [–]
R_{min} – minimum radius of the coil, [m]
R_{max} – maximum radius of the coil, [m]
r – radius of curvature, [m]
s – pipe wall thickness, [m]
T – fluid temperature, [K]
t – temperature, [°C]
U_i – velocity components, [ms^{-1}]
u_i – fluctuating velocity component, [ms^{-1}]
V – mean velocity, [ms^{-1}]

Greek symbols

δ – curvature ratio (= $d_i/2r$), [–]
θ – circumferential position, [°]
λ – thermal conductivity, [Wm^{-1}K^{-1}]
μ – dynamic viscosity, [Pa·s]
ρ – density, [kgm^{-3}]
φ – fluctuating part of temperature, [K].

Subscripts

av – average
crit – critical
in – inlet
ini – initial
out – outlet

References

[1] Dean, W. R., Note on the Motion of Fluid in a Curved Pipe, *Philosophical Magazine, 4* (1927), 20, pp. 208-223
[2] Dean, W. R., The Stream-Line Motion of Fluid in a Curved Pipe, *Philosophical Magazine, 5* (1928), 30, pp. 673-695
[3] Naphon, P., Suwagrai, J., Effect of Curvature Ratios on the Heat Transfer and Flow Developments in the Horizontal Spirally Coiled Tubes, *International Journal of Heat and Mass Transfer, 50* (2007), 3, pp. 444-451
[4] Balakrishnan, R*et al*., Heat Transfer Correlation for a Refrigerant Mixture in a Vertical Helical Coil Evaporator, *Thermal Science, 13* (2009), 4, pp. 197-206
[5] Rajavel, R., Saravanan, K., Heat Transfer Studies on Spiral Plate Heat Exchanger, *Thermal Science, 12* (2008), 3, pp. 85-90
[6] Naphon, P., Study on the Heat Transfer and Flow Characteristics in a Spiral-Coil Tube, *International Communications in Heat and Mass Transfer, 38* (2011), 1, pp. 69-74
[7] Khan, M. K., *et al*., Experimental Investigation on Diabatic Flow of R-134a through Spiral Capillary Tube, *International Journal of Refrigeration, 32* (2009), 2, pp. 261-271
[8] Naphon, P., Wongwises, S., An Experimental Study on the In-Tube Convective Heat Transfer Coefficients in a Spiral Coil Heat Exchanger, *International Communications in Heat and Mass Transfer, 29* (2002), 6, pp. 797-809
[9] Ho, J. C., Wijeysundera, N. E., Study of Compact Spiral-Coil Cooling and Dehumidifying Heat Exchanger, *Applied Thermal Engineering, 16* (1996), 10, pp. 777-790
[10] Ho, J. C., Wijeysundera, N. E., An Unmixed-Air Flow Model of a Spiral Coil Cooling Dehumidifying Unit, *Applied Thermal Engineering, 19* (1999), 8, pp. 865-883
[11] Nakayama, A., *et al*., Conjugate Numerical Model for Cooling a Fluid Flowing through a Spiral Coil Immersed in a Chilled Water Container, *Numerical Heat Transfer, Part A, 37* (2000), 2, pp. 155-165
[12] Kurnia, J. C., *et al*., Numerical Investigation of Laminar Heat Transfer Performance of Various Cooling Channel Designs, *Applied Thermal Engineering, 31* (2011), 6, pp. 1293-1304

[13] Alammar, K. N., Turbulent Flow and Heat Transfer Characteristics in U-Tubes: A Numerical Study, *Thermal Science*, *13* (2009), 4, pp. 175-181
[14] Yang, R., Chiang, F. P., An Experimental Heat Transfer Study for Periodically Varying-Curvature Curved-Pipe, *International Journal of Heat and Mass Transfer*, *45* (2002), 15, pp. 3199-3204
[15] Sasmito, A. P., *et al*., Numerical Evaluation of Laminar Heat Transfer Enhancement in Nanofluid Flow in Coiled Square Tubes, *Nanoscale Research Letters*, *6* (2011), 1, pp. 376-385
[16] Sasmito, A. P., *et al*., Numerical Analysis of Laminar Heat Transfer Performance of In-plane Spiral Ducts with Various Cross-Sections at Fixed Cross-Section Area, *International Journal of Heat and Mass Transfer*, *55* (2012), 21, pp. 5882-5890
[17] Vashisth, S., *et al*., A Review on the Potential Applications of Curved Geometries in Process Industry, *Industrial and Engineering Chemistry Research*, *47* (2008), 10, pp. 3291-3337
[18] Morton, B. R., Laminar Convection in Uniformly Heated Horizontal Pipes at Low Rayleigh Numbers, *Quarterly Journal of Mechanics and Applied Mathematics*, *12* (1959), 4, pp. 410-420
[19] Mori, Y., *et al*., Forced Convective Heat Transfer in Uniformly Heated Horizontal Tubes, *International Journal of Heat and Mass Transfer*, *9* (1965), 5, pp. 453-463
[20] Djordjević, M., *et al*., Numerical Analyses of the Radiant Heat Flux Produced by Quartz Heating System, *Proceedings*, The 3rd International Conference Mechanical Engineering in XXI Century, Nis, Serbia, 2015, pp. 75-80
[21] Patankar, S. V., *Numerical Heat Transfer and Fluid Flow*, Taylor & Francis, New York, USA, 1980
[22] Kays, W., *et al*., *Convective Heat and Mass Transport*, 4th ed., MacGraw Hill, Singapore, 2005
[23] ***, IAPWS Industrial Formulation for the Thermodynamic Properties of Water and Steam (IAPWS-IF97), The IAPWS-IF97, 2007
[24] Ali, S., Seshadri, C., Pressure Drop in Archimedean Spiral Tubes, *Industrial and Engineering Chemistry Process Design and Development*, *10* (1971), 3, pp. 328-332
[25] Piazza, I. Di, Ciofalo, M., Numerical Prediction of Turbulent Flow and Heat Transfer in Helically Coiled Pipes, *International Journal of Thermal Sciences*, *49* (2010), 4, pp. 653-663
[26] ***, ANSYS FLUENT Theory Guide, Release 15.0, ANSYS Inc., Canonsburg, Penn., USA, 2013
[27] ***, ANSYS FLUENT User's Guide, Release 15.0, ANSYS Inc., Canonsburg, Penn., USA, 2013
[28] Gnielinski, V., Heat Transfer and Pressure Drop in Helically Coiled Tubes, *Proceedings*, The 8th International Heat Transfer Conference, Vol. 6, Tayler and Francis, Washington, DC, 1986, pp. 2847-2854
[29] Seban, R. A., McLaughlin, E. F., Heat Transfer in Tube Coils with Laminar Turbulent Flow, *International Journal of Heat and Mass Transfer*, *6* (1963), 5, pp. 387-395
[30] Lin, C. X., Ebadian, M. A., Developing Turbulent Convective Heat Transfer in Helical Pipes, *International Journal of Heat and Mass Transfer*, *40* (1997), 16, pp. 3861-3873

Paper submitted: March 21, 2016
Paper revised: September 30, 2016
Paper accepted: October 10, 2016